



**HAL**  
open science

## Vectorial dispersive shock waves in optical fibers

Javier Nuño, Christophe Finot, Gang Xu, Guy Millot, Miro Erkintalo, Julien Fatome

► **To cite this version:**

Javier Nuño, Christophe Finot, Gang Xu, Guy Millot, Miro Erkintalo, et al.. Vectorial dispersive shock waves in optical fibers. *Communications Physics*, 2019, 2, pp.138. 10.1038/s42005-019-0241-6 . hal-01821862v2

**HAL Id: hal-01821862**

**<https://hal.science/hal-01821862v2>**

Submitted on 6 Nov 2019

**HAL** is a multi-disciplinary open access archive for the deposit and dissemination of scientific research documents, whether they are published or not. The documents may come from teaching and research institutions in France or abroad, or from public or private research centers.

L'archive ouverte pluridisciplinaire **HAL**, est destinée au dépôt et à la diffusion de documents scientifiques de niveau recherche, publiés ou non, émanant des établissements d'enseignement et de recherche français ou étrangers, des laboratoires publics ou privés.



# COMMUNICATIONS PHYSICS

## ARTICLE

<https://doi.org/10.1038/s42005-019-0241-6>

OPEN

# Vectorial dispersive shock waves in optical fibers

J. Nuño<sup>1,2</sup>, C. Finot <sup>1</sup>, G. Xu<sup>1</sup>, G. Millot<sup>1</sup>, M. Erkintalo<sup>3,4</sup> & J. Fatome<sup>1\*</sup>

Dispersive shock waves are a universal phenomenon encountered in many fields of science, ranging from fluid dynamics, Bose-Einstein condensates and geophysics. It has been established that light behaves as a perfect fluid when propagating in an optical medium exhibiting a weakly self-defocusing nonlinearity. Consequently, this analogy has become attractive for the exploration of dispersive shock wave phenomena. Here, we observe of a novel class of vectorial dispersive shock waves in nonlinear fiber optics. Analogous to blast-waves, identified in inviscid perfect fluids, vectorial dispersive shock waves are triggered by a non-uniform double piston imprinted on a continuous-wave probe via nonlinear cross-phase modulation, produced by an orthogonally-polarized pump pulse. The nonlinear phase potential imparted on the probe results in the formation of an expanding zone of zero intensity surrounded by two repulsive oscillating fronts, which move away from each other with opposite velocities.

<sup>1</sup>Laboratoire Interdisciplinaire Carnot de Bourgogne, UMR 6303 CNRS-Université Bourgogne-Franche-Comté, 9 av. A. Savary, Dijon, France. <sup>2</sup>Now at Departamento de Electrónica, Universidad de Alcalá, 28805 Alcalá de Henares, Madrid, Spain. <sup>3</sup>The Dodd-Walls Centre for Photonic and Quantum Technologies, Auckland, New Zealand. <sup>4</sup>Department of Physics, The University of Auckland, Auckland 1010, New Zealand. \*email: [julien.fatome@u-bourgogne.fr](mailto:julien.fatome@u-bourgogne.fr)

The formation of dispersive shock waves (DSWs) is a fundamental mechanism encountered in many fields of science, such as hydrodynamics, geophysics, atmospheric science, socioeconomics, chemistry, acoustics, quantum fluids, and nonlinear optics<sup>1–28</sup>. One of the most fascinating manifestations of DSWs in nature is the appearance of the popular mascaret wave, which can be generated in specific river estuaries due to a counter-flow between tide and current, resulting in the formation of large undular tidal bores traveling up-stream. This phenomenon is particularly well-appreciated by the surfing community<sup>1,2</sup>. Another spectacular manifestation of DSWs in atmospheric air-flow is the emergence of Morning Glory roll clouds and mountain waves<sup>3</sup>. In general, DSW phenomena occur in conservative (or weakly dissipative) non-viscous systems, and they rely on two fundamental ingredients: nonlinearity and wave dispersion. The most common situation involves the dispersive regularization of a step-like initial condition (in amplitude or velocity)—an example of the so-called Riemann problem—and gives rise to the expansion of non-stationary oscillating fan structures connecting both upper and lower initial non-oscillating states<sup>5–7</sup>. Because of their universal role in counteracting unphysical singularities in dispersive conservative media, DSW prototypes have become the subject of intense research in physics, with groundbreaking results obtained in diverse areas ranging from fluid dynamics to two-component Bose-Einstein condensates (BEC)<sup>6–11,23–28</sup>.

DSWs have also been observed and extensively studied in the context of nonlinear optics<sup>10–22</sup>. In particular, it is well-known that light behaves as an ideal inviscid perfect fluid in an optical medium that exhibits a weakly self-defocusing Kerr nonlinearity<sup>11,18–21</sup>. Accordingly, the propagation of light through such a medium can be modeled using shallow water wave Euler equations, which predict that any initial modulations experience a strong steepening that leads to the formation of a gradient catastrophe and subsequently DSWs<sup>6,7,19–21,29</sup>. This analogy has attracted significant attention, as it highlights the elegant prospect of using nonlinear optical systems as convenient laboratory testbeds for the exploration of universal DSW physics.

Ever since the pioneering work by Rothenberg and co-workers in optical fibers about two decades ago<sup>10</sup>, tremendous efforts have been dedicated to develop powerful testbed platforms, which are capable of mimicking fluid-type DSWs with nonlinear optics<sup>11–18</sup>. Unfortunately, despite extensive attempts, the experimental generation and characterization of pure optical DSW remain challenging. In the vast majority of previous works, the DSWs are generated through the nonlinear steepening of an intense bright pulse superimposed on a continuous-wave (CW) background propagating in a self-defocusing nonlinear Kerr medium<sup>17,22</sup>. Due to self-phase modulation, the high-intensity gradient region of the pulse generates new frequencies, which then disperse onto the plane-wave background creating an interference pattern that triggers the formation of DSWs<sup>7,11,17</sup>. Although such experimental configurations have enabled valuable insights into DSW dynamics, they share a common deficiency: the CW landscape and the intense pump share a common optical mode. Because of this issue, a significant part of the physical information encoded on the CW landscape is hidden by the intense pump pulse itself, preventing its examination. Therefore, neither blast-waves (sudden disturbances creating a sharp area of supersonically expanding pressure or density), nor pistons or DSW collision problems can be emulated<sup>6–9,30–34</sup>. To overcome these issues, one has to dissociate the DSW formation from the initial high intensity pump in such a way as to imprint the dispersive hydrodynamics phenomenon only on the CW landscape. An easy-to-implement laboratory platform capable of such dissociation would dramatically expand the DSW phenomena that can be

investigated, enabling for instance the study of blast-wave dynamics, complex piston problems, and the full emulation of a supersonic object (in the sense that it travels faster than the “speed of sound” within the medium), moving in a purely dispersive fluid<sup>11,30,35</sup>.

In this contribution, we propose and experimentally demonstrate a novel nonlinear optical scheme that allows for the full isolation of DSW dynamics. Our approach leverages the two orthogonal polarizations supported by silica glass optical fibers: an intense pump pulse acts as a moving piston that imprints a nonlinear phase shift through cross-phase-modulation (XPM) on an orthogonally polarized CW probe that is co-propagating in a normally dispersive optical fiber, resulting in the generation of two DSWs that are moving away from each other. More specifically, thanks to the orthogonal polarizations of the CW landscape and the intense piston pulse, the DSW dynamics can be straightforwardly isolated, permitting direct experimental observation of a depletion zone induced by two repulsive piston shock effects. Almost 30 years after the pioneering work of Joshua E. Rothenberg reporting the observation of wave-breaking induced buildup of modulational instability in a birefringent optical fiber<sup>36</sup>, our results represent the experimental observation of vectorial DSWs in nonlinear optics. Finally, we have also investigated how group-velocity mismatch between the CW landscape and the piston pulse impacts the DSW dynamics. Our work provides significant insights on the mechanism for the generation of DSWs and demonstrates a convenient platform that allows for the systematic and detailed experimental study of DSW physics.

## Results

**Modeling and principle of operation.** As schematically illustrated in Fig. 1, the system under study exploits the vectorial XPM interaction between a weak CW probe and an orthogonally polarized intense short pulse, both propagating within a normally dispersive optical fiber.

In the framework of nonlinear fiber optics<sup>37</sup>, the evolution of the complex slowly varying amplitudes of the pump pulse  $u(z,t)$  and the CW probe  $v(z,t)$  are described by a set of two coupled nonlinear Schrödinger (NLS) equations. In standard optical fibers, random longitudinal fluctuations of the residual birefringence occur along the fiber in a length-scale of a few meters. Averaging out the nonlinear contribution over these fast polarization fluctuations in km-long fibers leads to the so-called Manakov model<sup>38,39</sup>:

$$\begin{cases} i \frac{\partial u}{\partial z} + \frac{\beta_2}{2} \frac{\partial^2 u}{\partial t^2} + \frac{8}{9} \gamma (|u|^2 + |v|^2) u + i \frac{\alpha}{2} u = 0, \\ i \frac{\partial v}{\partial z} + i \delta \frac{\partial v}{\partial t} + \frac{\beta_2}{2} \frac{\partial^2 v}{\partial t^2} + \frac{8}{9} \gamma (|u|^2 + |v|^2) v + i \frac{\alpha}{2} v = 0 \end{cases} \quad (1)$$

here,  $z$  and  $t$  denote the propagation distance coordinate and time in the co-moving frame of the piston pump pulse, respectively.  $\gamma$  corresponds to the nonlinear Kerr parameter of the fiber,  $\beta_2$  is the group velocity dispersion coefficient, and  $\alpha$  indicates propagation losses. The corrective factor of 8/9 is applied to the Kerr effect due to the polarization randomness assumed in the Manakov model. The term  $\delta = 2\pi \beta_2 \delta f$  describes the walk-off

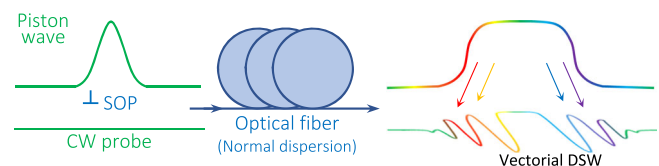


**Fig. 1** Principle of operation. Schematic of the vectorial dispersive shock wave phenomenon

between the pulse and the CW landscape when the central frequencies of the two waves are separated by a small frequency offset  $\delta f$ . Let us stress that no transfer of energy occurs between the two waves during the nonlinear interaction. Indeed, it should be clear from Eq. (1) that the two waves are only coupled by a phase term, which is proportional to the intensity of the waves. Accordingly, the energy initially contained in the CW probe (or piston pulse) remains unchanged (except for linear losses). Note that we neglect higher-order effects such as third-order dispersion, self-steepening and Raman scattering, as they have been found to play a negligible role in the present dynamics. This assumption is verified *a posteriori* by the excellent agreement between our experimental observations and numerical modeling.

In terms of fluid-like or condensate variables, the set of coupled NLS equations above can be cast into their hydrodynamic forms by means of the well-known Madelung transformation<sup>6,9,11,18</sup> (see Supplementary notes 1 and 2). In this configuration, the intensity and the gradient of the phase (chirp profile) assume respectively the roles of the density and velocity of the fluid. It then turns out that the exchange of momentum during the shock process is here induced by the XPM coupling term which acts as a sharp defocusing potential for the fluid. In a sense, our experiment constitutes the 1-D counterpart of the “blast-wave” or double piston shock problem already studied in quantum superfluid and induced by a laser beam<sup>9,11,31,32</sup>. The background density which sets the reference speed of sound is here dictated by the intensity level of the CW landscape, while strong density perturbations (here the high-power pump beam) naturally correspond to supersonic sources<sup>11,23</sup>.

**Dynamics of the vectorial dispersive shock wave.** We begin by numerically illustrating the formation and evolution of vectorial DSWs. To this end, we consider the following set of parameters which mimics the experiments that will follow. The piston pump wave is a Gaussian-like chirp-free pulse with the following characteristics: temporal half-width at  $1/e$  of its maximum intensity  $t_0 = 41$  ps, peak power  $P_c = 1.5$  W and central wavelength  $\lambda_p = 1550$  nm. The orthogonally polarized CW probe propagates with the same group velocity as the piston beam ( $\delta f = 0$ ) and its average power is set to be 5 mW. The normally dispersive fiber is a 13-km-long dispersion compensating fiber (DCF) typically used in the field of dispersion managed data transmission (for parameters, see Methods). It is important to emphasize that the above physical parameters place our problem in the weakly dispersive regime of the NLS (at least in the initial stage of propagation), for which the ratio between the nonlinear and dispersive effects—given by the usual soliton number  $N$ —is much larger than unity (see Supplementary note 3 for more discussions dealing with the balance between nonlinear and dispersive effects along the propagation distance, as well as Supplementary note 4 for the influence of the CW probe power). Indeed, with the maximum pump power in our experiments, we have  $N = \sqrt{L_d/L_{nl}} = \sqrt{\gamma' P_c t_0^2 / \beta_2} \sim 14$ <sup>37</sup>, where  $\gamma' = 8 \gamma / 9$ . Accordingly, the analogy between nonlinear optics and shallow water hydrodynamics is fully appropriate for our study, at least in the early stage of propagation (see the Supplementary notes 1 and 2 for further details on the analogy).

Figure 2 shows numerically simulated dynamics of vectorial DSW generation. These simulations were obtained through the numerical integration of Eq. (1) by means of the split-step Fourier algorithm<sup>37</sup>. Note also that for clarity, the XPM coupling term arising from the probe and acting on the pump wave is perturbative and can be neglected to first order in Eq. (1). Focusing first on the piston field  $u(z,t)$  [Fig. 2a, b], we see dynamics typical for an intense pulse propagating in a defocusing

Kerr medium<sup>40,41</sup>. The initial stages of the evolution are dominated by self-phase-modulation, which gives rise to strong spectral broadening [cf. Fig. 2a]. This initial spectral broadening ceases at the so-called wave breaking distance  $z_c$  at which point the spectral width reaches the maximum value of  $\Delta f_{\max}$ . Both  $z_c$  and  $\Delta f_{\max}$  can be accurately estimated using theories of the ubiquitous wave-breaking phenomenon<sup>40,41</sup> (more details on the following formulas are given in the Supplementary note 5):

$$z_c \simeq \frac{1.61 t_0}{\sqrt{\beta_2 \gamma' P_c}} \quad (2)$$

$$\Delta f_{\max} = \frac{1}{2^{1/4} \pi} \sqrt{\frac{\gamma' P_c}{\beta_2}} = \frac{N}{2^{1/4} \pi t_0} \quad (3)$$

As shown with the cyan dashed-line and open circles in Fig. 2a, these estimates are in good agreement with our simulations.

Following the initial stage of spectral broadening, chromatic dispersion dominates, resulting in strong temporal expansion [Fig. 2b]. In accordance with the principles of dispersive Fourier transform<sup>42–44</sup>, the piston pulse spectrum maps into the temporal domain during propagation; in the far-field, both the spectral and temporal profiles of the pulse exhibit similar parabolic profiles<sup>42,45</sup>. The maximal temporal width  $\Delta t_{\max}$  of the piston pulse at position  $z$  can be estimated by:

$$\Delta t_{\max} = 2^{3/4} z \sqrt{\gamma' P_c \beta_2} \simeq 2.71 t_0 z / z_c \quad (4)$$

As highlighted with the dashed white lines in Fig. 2b, this expression agrees very well with the temporal expansion of the piston pulse observed in our numerical simulations.

Let us now consider the CW probe beam  $v(z,t)$ . In the initial stage of evolution (during which the piston pulse temporal profile stays almost constant), XPM coupling gives rise to a non-uniform nonlinear phase shift that increases linearly with propagation  $\phi_{nl}(z,t) \sim \gamma' |u(0,t)|^2 z$ <sup>46</sup>. As evidenced by the strong spectral broadening of the probe beam [Fig. 2c], this nonlinear phase shift gives rise to an instantaneous frequency shift (chirp)  $\delta\omega(z,t) = -\partial_t \phi_{nl}(z,t) = -\gamma' \partial_t |u(0,t)|^2 z$  across the CW landscape: the region overlapping with the leading (trailing) edge of the piston pulse is redshifted (blueshifted). Since blue light travels slower than red light in normally dispersive media, this chirp manifests itself in the temporal domain as an instantaneous change of velocity  $V$  around the central portion of the probe/piston pulse, with  $\delta V(z,t) \propto -\beta_2 \delta\omega(z,t)$ . We consequently observe the emergence of two fronts with opposite velocities that are traveling away from each other, as well as the concomitant removal of energy (decompression of photons) from the central region defined by the initial piston pulse [see Fig. 2d]. With subsequent propagation, chromatic dispersion begins to regulate the steep edges of the fronts (compression), giving rise to the development of fast non-stationary oscillations surrounding a temporal gap—a characteristic imprint of double piston DSW<sup>7,9,33</sup>. We identify the present dynamics to belong in the “slow piston regime” as defined by Hofer et al.<sup>31</sup>, which means that the initial group velocity jump imposed by the piston wave is moderate. Indeed, we do not observe any vacuum state in the oscillations and the two DSWs are not connected. However, we attribute the absence of a plateau area usually induced by the classical double piston shock problem to the development of both rarefaction waves in the center of the probe via the action of XPM decompression (see Supplementary notes 1 and 2 for more details dealing with the hydrodynamic description of this vectorial DSW phenomenon, as well as Supplementary notes 6 for the key role of the XPM coupling coefficient). On the other hand, the overall dynamics can be very

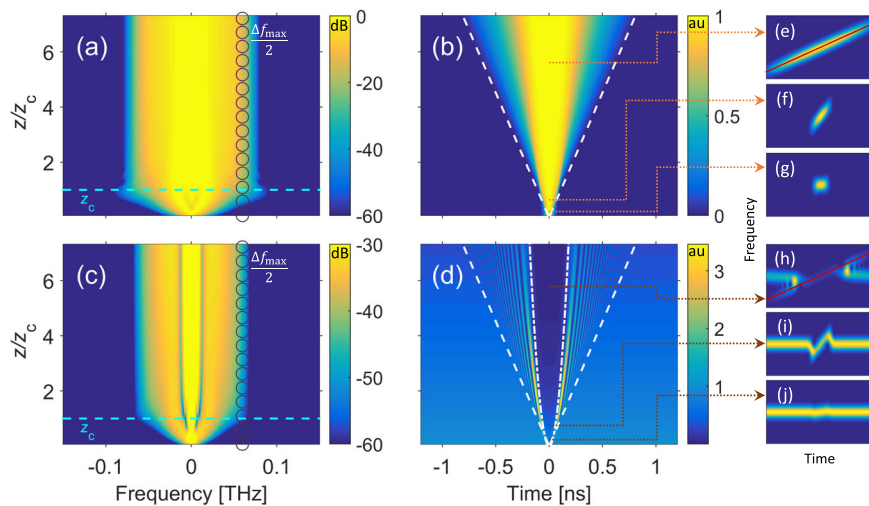


**Fig. 2** Illustrative numerical simulations. **a** Longitudinal evolution of the spectrum of the piston pulse. The cyan dashed-line indicates the distance  $z_c$  predicted by Eq. (2) (1.8 km), while the open circles highlight  $\Delta f_{\max}/2$  predicted by Eq. (3). **b** Longitudinal evolution of the temporal intensity profiles of the piston pulse (normalized to its maximum); au: arbitrary unit. **c** Same as **(a)** for the probe wave. **d** Longitudinal evolution of the temporal intensity profiles of the probe wave (normalized to the continuous wave background). In panels **(b)** and **(d)**, analytical predictions of the temporal expansion provided by Eqs. (4) and (5) are plotted using white dashed-line and dash dotted-line, respectively. The simulation results are obtained using parameters corresponding to our experiments (see Methods) and for a pulse peak power of 1.5 W. **e–g** Spectrograms of the piston pulse at  $z = 0.05, 0.7$  and  $5.6 z_c$ , respectively. **h–j** Corresponding spectrograms of the probe wave. The spectrograms are plotted on a linear scale and extend from  $-300$  ps to  $300$  ps (horizontal axis) and from  $-80$  GHz to  $80$  GHz (vertical axis). The red lines in panels **(g)** and **(j)** indicate the far field chirp profile of slope  $1/(\beta_2 z)$

well captured when illustrating the evolution of the probe beam by means of a spectro-temporal approach<sup>47,48</sup>. To this aim, we have displayed in Fig. 2e–g, h–j, the spectrograms of the piston and probe waves at  $z = 0.05, 0.7$ , and  $5.6 z_c$ , respectively. As can be observed, the piston pulse experiences a large temporal and spectral expansion, while the interplay between dispersion and nonlinearity subsequently induces, after the wave breaking distance  $z_c$ , a close-to-linear chirp with a slope given by  $1/(\beta_2 z)$ , indicated with red lines in panels **(g)** and **(j)**<sup>42</sup>.

The dynamics of the cw probe is markedly more complex than the dynamics of the pump. Because of the XPM coupling, the piston beam induces on the CW landscape a chirp profile proportional to the gradient of its intensity profile. Note in particular that, during the early stage of propagation (Fig. 2i at  $z = 0.7 z_c$ ), a typical N-wave shape of the chirp profile forms through a process analogous to the formation of a pressure wave occurring during a supersonic boom event<sup>30,49</sup>. Then, as the piston pulse expands and develops steeper and steeper edges, the redshifted and blueshifted parts of the probe are pushed away from the center due to chromatic dispersion, creating a temporal gap which continuously expands over propagation. On both sides of this rarefaction area, a DSW emerges from the fast oscillations occurring between the remaining continuous wave background and new frequencies<sup>17</sup>.

Because the nonlinear phase imparted on the probe beam is dominated by XPM, Eqs. (2–4) also apply when describing the temporal and spectral spreading of the DSW, as shown in Fig. 2c, d. Here, it is worth emphasizing that Eq. (4) in particular captures the universal fact that the rate of expansion of a DSWs is a square-root function of the medium density, portrayed in our optical system by the intensity jump<sup>6,9,35</sup>. Moreover, we note that, when plotted versus the normalized distance  $z/z_c$ , the shock cone imposed by the piston pulse is only determined by the sharpness of the source, i.e.,  $t_0$ . That is to say, the angle of the white dashed-lines cone is simply provided by  $\tan^{-1}(2.71 t_0)$ .

By considering the peak power reduction of the piston pulse due to temporal broadening along the propagation distance and neglecting fiber losses, we can also derive an estimate for the

rarefaction area  $\Delta t_{\min}$  that describes the width of the temporal gap created within the probe landscape:

$$\Delta t_{\min} = 2^{3/4} z \sqrt{\gamma P_{\min} \beta_2} \quad (5)$$

where

$$P_{\min} = P_c \frac{t_0}{\Delta t_{\max}} \quad (6)$$

As highlighted with the dash dotted white line in Fig. 2d, this estimate of  $\Delta t_{\min}$  agrees well with our simulation results and illustrates the fact that the rate of expansion of the rarefaction area is not constant but rather decelerates with propagation.

**Experimental setup.** To experimentally generate and observe such vectorial DSWs, we have implemented the setup depicted in Fig. 3a [see Methods for additional details]. 68-ps Gaussian-like optical pulses are first generated by intensity modulating a 1550 nm CW laser. This pulse train is then amplified using an Erbium doped fiber amplifier (EDFA) and used as the piston pump wave. The probe wave consists of a 5-mW CW which can be generated at the same central wavelength as the piston pulse or at a distinct wavelength to explore the effect of a variable velocity mismatch between the piston and the probe signals. Both waves are then orthogonally polarized using a polarization beam splitter (PBS), and injected into a 13-km-long segment of normally dispersive compensating fiber (see Methods for detailed parameters). At the output of the system, the piston and the probe waves are polarization demultiplexed and subsequently characterized in the temporal and spectral domains. Note that this experimental testbed platform relies exclusively on commercial devices widely used in the telecommunication industry, and that the all-fibered nature of the setup ensures stable operation for several consecutive hours.

**Experimental observation of vectorial DSWs.** Figure 3b shows experimentally measured DSW dynamics when a single CW laser is used for both the piston pulse and the probe wave (null

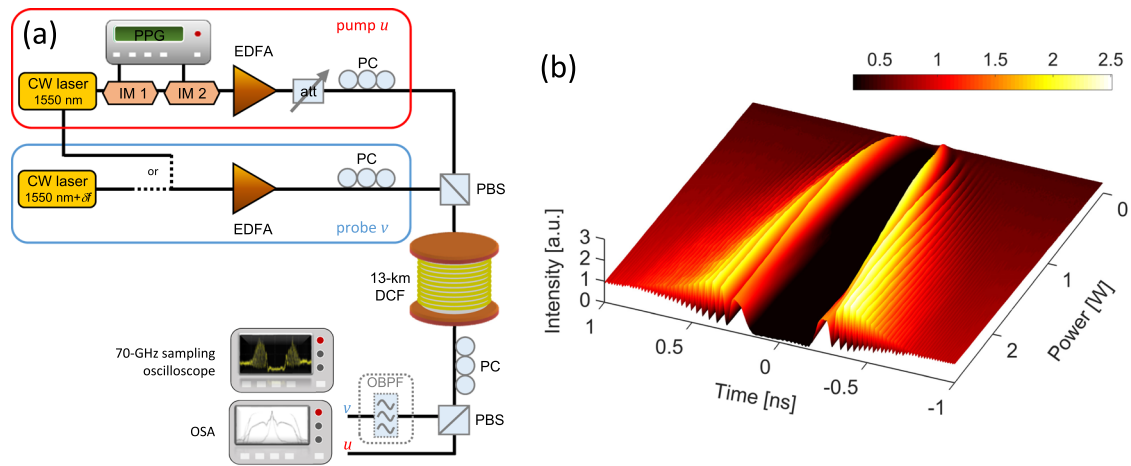


**Fig. 3** Experimental setup and illustrative observations of vectorial dispersive shock wave dynamics. **a** Experimental setup: CW Continuous Wave, PPG Pulse Pattern Generator, IM Intensity Modulator, EDFA Erbium Doped Fiber Amplifier, Att Optical Attenuator, PC Polarization Controller, PBS Polarization beam splitter, DCF Dispersion Compensating Fiber, OBPB Optical BandPass Filter, OSA Optical Spectrum Analyzer. **b** False-color plot showing the experimentally recorded evolution of the output intensity profile of the probe beam as a function of the input piston pulse peak power (a. u.: arbitrary unit). Data values are normalized with respect to the CW landscape equal to 1 and mapped to colors linearly

walk-off configuration,  $\delta f = 0$ ). Specifically, here we depict the probe beam intensity profile recorded on our sampling oscilloscope for a range of piston powers. (Note that varying the piston peak power at constant fiber length yields similar insights as recording the longitudinal evolution of the fields at maximum power, but avoids the use of a destructive cutback method). In accordance with the qualitative description presented above, we see very clearly that the CW landscape of the probe beam is broken by two repulsive fronts imposed by the double piston effect. As the piston peak-power increases (and the shock becomes more abrupt), the oscillations in the tails of the fronts increase in frequency. This process is analogous to the 1-D behavior of blast DSWs created by a laser beam injected through a quantum fluid or BEC<sup>9</sup>, with the defocusing potential imposed in our system by the pump-induced XPM.

Our experimental observations are in quantitative agreement with theoretical predictions and numerical modeling, as shown in Fig. 4. Here we compare the experimentally measured intensity profiles of the probe [Fig. 4a] and piston [Fig. 4b] beams as a function of the piston pulse peak power with corresponding results from numerical simulations [Fig. 4c,d]. The agreement between our experiments and simulations is remarkable. We emphasize that no free-running fitting parameters were used: the simulations make exclusive use of experimental parameters. Moreover, as highlighted by the white dashed curves and dash-dotted lines in Fig. 4, we see how the experimentally-resolved dynamics of the DSW process (e.g., width of the gap region in the probe wave and the width of the piston pulse beam) agrees extremely well with the analytical predictions based on Eqs. (4) and (5).

To gain further insights, Fig. 5 shows a comprehensive input-output analysis of the piston and probe waves for an injected pulse peak-power of 1.5 W. First, Fig. 5a compares the input and output intensity profiles of the piston pulse, revealing the large temporal broadening that takes place in the DCF: the half-width of the piston pulse increases from 68 ps (blue solid line) to more than 1.4 ns (yellow line). As highlighted by the open circles, we also see that the profile of the output pulse can be very well approximated with a parabolic profile of width  $\Delta t_{\max}$  given by Eq. (4). However, small oscillations that deviate from the parabolic shape are visible on the edges of the pump profile. These

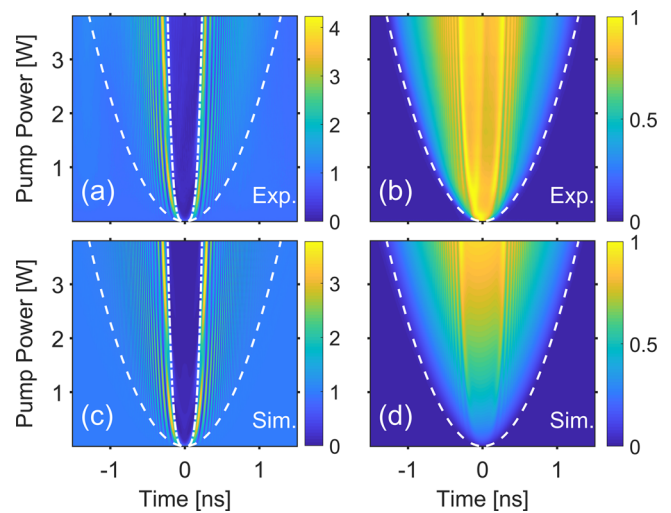


**Fig. 4** Comparison between experimental, theoretical, and numerical results. **a, b** Pseudo-color plots depicting the evolution of the output temporal intensity profile of the **(a)** probe wave and **(b)** the piston beam as a function of the injected piston peak-power. **c, d** Corresponding numerical simulation results. For the probe panels, data values are normalized by the level of the continuous wave landscape, while the piston panels are normalized by the maximum available peak power. The white dashed lines and dash-dotted lines highlight theoretically predicted dynamics of the shock expansion based on Eqs. (4) and (5), respectively

oscillations originate from the back-action of the DSW on the piston pulse through XPM, as confirmed by the fact that no oscillation is observed when only the pulse propagates through the fiber (magenta solid curve).

Figure 5b compares the input and output intensity profiles of the probe wave. Here the dramatic transformation of the CW landscape into a blast-like DSW can be readily observed. Indeed, the output intensity profile is characterized by a wide-open temporal gap surrounded by two strongly modulated wave trains. We must emphasize that the oscillating fan structure of the fronts can be fully resolved in our system, underlining its potential to

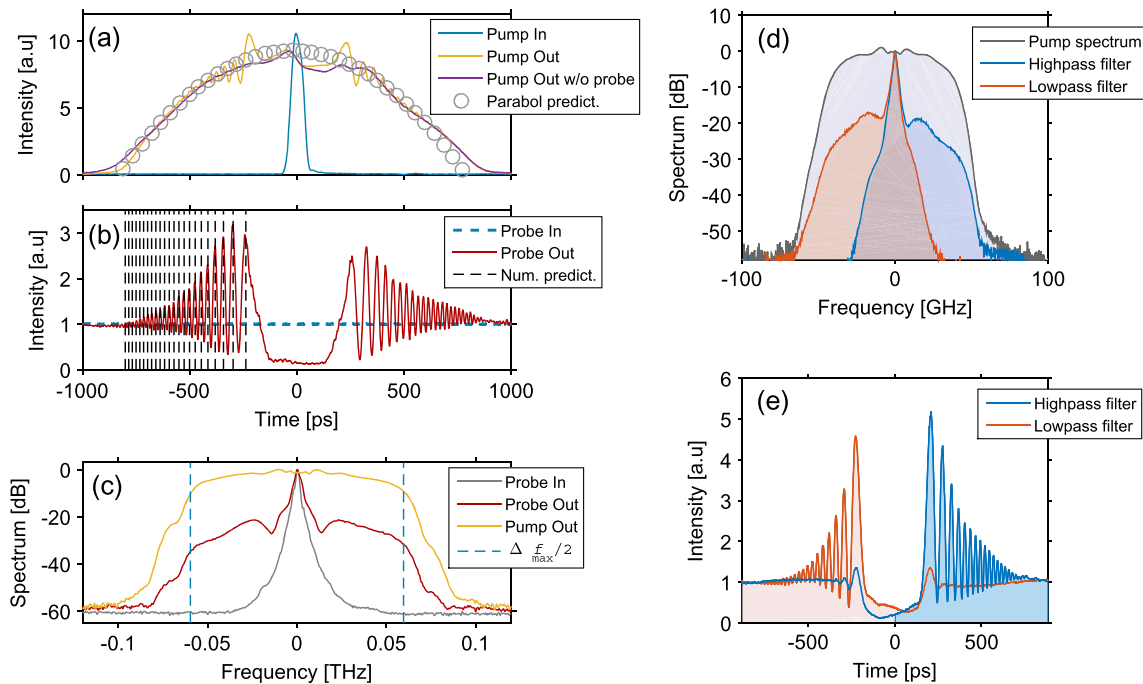


**Fig. 5** Input-output comparison of the piston pulse and probe wave for a peak power of 1.5 W. **a** Blue solid line shows the input temporal profile of the piston pulse, while the yellow and purple lines show the corresponding output profiles in the presence and absence of the continuous wave probe, respectively. Open circles correspond to a parabolic profile of width  $\Delta t_{f_{\max}}$ . (a. u.: arbitrary unit). **b** Temporal profile of the probe wave at the fiber input (blue dashed line) and output (red solid line). Vertical black dashed lines indicate the positions of the oscillation maxima predicted by numerical simulations based on Eq. (1). Note that, in panel (b), data values are normalized with respect to the output CW landscape, while in panel (a) an arbitrary normalization is used for convenience and clarity. **c** Experimental spectra of the initial and output probe beam compared to the output pump spectrum. Theoretical prediction of the maximum spectral expansion  $\Delta f_{\max}$  is also displayed with blue dashed lines. Note that the measured spectrum of the injected pump wave coincides with the initial probe spectrum since both signals are generated from the same CW laser source. **d–e** Spectro-temporal characterization of vectorial dispersive shock waves. **d** Experimental output spectrum after optical filtering obtained for a piston pulse peak power of 1 W. **e** Output temporal intensity profile of the probe signal after spectral filtering. Resulting profile in red (blue), when only the low (high) frequencies are conserved

provide exquisitely detailed insights into DSW dynamics. Moreover, the absence of any major asymmetry, typically caused by e.g., third-order dispersion, self-steepening or Raman scattering, confirms the purity of the system. Indeed, the small amplitude asymmetry observed between the two DSW is attributed to the small asymmetry of the input pulse which can be mitigated by further optimization. It is interesting to note that the oscillations displayed by the DSWs are chirped, i.e., their period is changing, in agreement with classical regularization of DSW<sup>6</sup>. This feature is fully reproduced by our numerical simulations, as shown by the vertical dashed lines in Fig. 5b, which highlight the positions of the oscillation maxima extracted from our simulations. As illustrated in Supplementary Fig. 7, this feature can be readily explained in terms of the dispersion-induced spectro-temporal mapping of the DSW.

Figure 5c compares the input and output spectral profiles of the probe and piston pulse beams. As can be seen, both waves undergo significant spectral broadening, characterized by an output total spectral expansion above 150 GHz—a value very close to the theoretical prediction  $\Delta f_{\max}$  (blue dashed lines). In this context, it is worth noting that the piston pump and the probe spectra exhibit very similar profiles, underlining the fact that XPM dominates the nonlinear evolution of the probe. We must also emphasize that, in accordance with the theoretical description presented above [see spectrograms in Fig. 2], the different spectral components of the probe beam are temporally segregated amongst the two DSWs, with redshifted

(blueshifted) frequency components associated with the leading (trailing) edge of the DSW. We have experimentally confirmed this feature by recording the spectral and temporal intensity profiles of the probe beam after it has passed through a 1-nm optical bandpass filter off-set from the 1550 nm center wavelength. Results are shown in Fig. 5d, e, and they readily show that filtering induces a striking asymmetry in the temporal intensity profile. Indeed, by filtering the output spectrum of the probe, we are able to annihilate half of the shock. More precisely, after canceling the higher frequencies (red curves), the temporal fan recorded for  $t > 0$  vanishes. In contrast, when higher frequencies and the continuous component are preserved (blue curves), the leading fan disappears. In both cases, the central hole still occurs since no energy is present in this part of the shock.

**Influence of a velocity mismatch.** Before concluding, we discuss the impact of relative walk-off between the probe and the piston beams. In this case, the DSW is triggered by a pulse that is moving relative to the CW landscape (in analogy with a counter-flow or over-flow collisions), resulting in asymmetric DSW dynamics. To experimentally engineer such a scenario, we create the piston pulse and the probe beams using two separate lasers with an adjustable frequency offset  $\delta f$ . (This should be contrasted with the experiments reported in the preceding section that only used a single laser.) Thanks to group-velocity dispersion, the probe and the piston

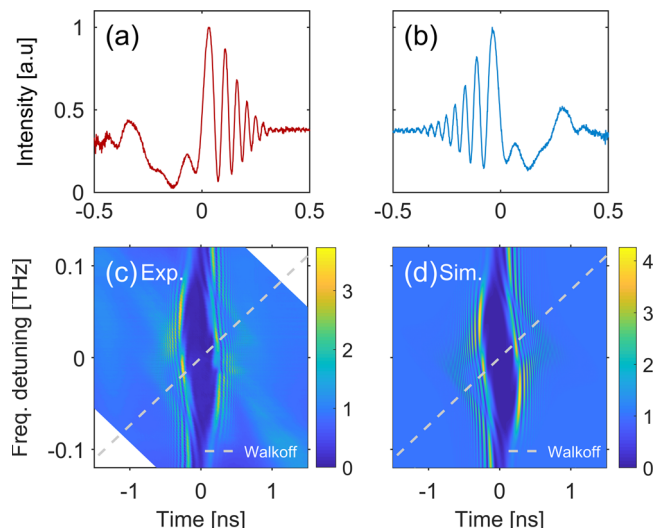


**Fig. 6** Influence of a velocity mismatch. **a, b** Temporal intensity profile of the probe beam at the fiber output for an offset frequency of **(a)**  $\delta f = 100$  GHz and **(b)**  $\delta f = -100$  GHz. **c** Experimentally measured output intensity profile of the probe wave as a function of frequency detuning  $\delta f$ . **d** Corresponding simulation results. Data in **(c)** and **(d)** are normalized by the level of the continuous wave intensity landscape. The dashed line shows the relative position of the piston pulse center (initially at zero) at the fiber output

beams travel with slightly different (group) velocities through the fiber, while nonlinearly interacting through XPM.

In Fig. 6a, we show the temporal intensity profile of the probe beam at the fiber output, when the piston pulse peak power is set to 2 W and the frequency offset  $\delta f = 100$  GHz (corresponding to a counter-flow configuration with a total walk-off of 1.29 ns over the 13-km-long fiber). We see clear signatures of asymmetric DSW dynamics, with an enhanced fan structure observed exclusively on the trailing part of the shock. By inverting the sign of the frequency offset ( $\delta f = -100$  GHz), the asymmetry is correspondingly inverted, with a clear fan structure on the leading part of the shock [see Fig. 6b]. A more comprehensive picture of the effect of relative walk-off is provided in Fig. 6c, where we show the probe beam intensity profile at the fiber output over a wide range of frequency offsets. Also shown as the dashed line is the trajectory of the piston pulse (i.e., the temporal position of the pump pulse center at the fiber output), which precisely follows the dispersive walk-off imposed by the frequency offset between the two waves. As expected, the shock waves vanish when the group-velocity difference between the two beams becomes larger than the expansion speed of the shock—dictated by the maximum frequency chirp (here around 70 GHz). These experimental results are again in excellent agreement with the corresponding numerical simulations, shown in Fig. 6d. Note finally that, in contrast to previous works<sup>50,51</sup>, which involve two high-density or high-power counter-flow components propagating in the defocusing regime of NLS, here no modulational instability process has been observed between the two orthogonal waves, essentially because of the strong power imbalance between the two components.

## Discussion

In conclusion, we have reported on the experimental demonstration of vectorial dispersive shock waves in the context of nonlinear fiber optics. Our scheme leverages the nonlinear XPM interaction between a weak CW probe co-propagating in

a normally dispersive optical fiber and an orthogonally polarized intense piston pulse. In contrast to previous studies, which have exclusively operated in the scalar regime, our system enables the generation of DSWs in a two-component vectorial configuration. Since the generated DSW is orthogonally polarized with respect to the intense piston beam, it can be fully isolated and characterized without being obscured by the pump pulse. Using this scheme and the correspondence between nonlinear optics and non-viscous hydrodynamics, we have been able to realize an optical analog of a double piston DSWs induced by a supersonic object moving across a superfluid-like medium, as characterized by the appearance of two repulsive, rapidly oscillating fronts surrounding a region of zero intensity. All our experimental observations are in excellent agreement with numerical simulations of the celebrated Manakov model, and they adhere to simple analytical guidelines predicted from established theories of wave breaking and spectro-temporal mapping induced by chromatic dispersion.

We anticipate that the presented results will stimulate analytical and statistical research that is above the scope of the present paper. We have shown how the piston pulse drives the evolution towards the shock and continuously affects its evolution; future works may for example focus on how the use of a chirped piston pulse could be beneficial to control the longitudinal evolution of the probe wave and associated DSWs. More generally, shock wave phenomena are often difficult to study in their natural environment, and also hard to reproduce in laboratory. Therefore, we believe that the present numerical and experimental research fully demonstrates that fiber optics may constitute a remarkable testbed platform for the experimental characterization of DSWs. Moreover, in contrast to numerous other implementations, our fiber-based vectorial approach constitutes a new avenue to non-destructively produce and study complex DSW phenomena such as blast-waves, non-uniform piston problems or ballistic impacts, by means of a compact, highly stable and high reproducible system. We therefore expect that other fields of physics involving two component interactions may be inspired by this research<sup>52</sup>.

## Methods

**Additional details on the experimental setup.** Further details are given with reference to Fig. 3. The testbed platform involved in the observation of vectorial DSW is all-fibered and relies exclusively on commercial devices widely used in the telecommunication industry. First-of-all, a train of 68-ps pulses at a repetition rate of 312.5 MHz is generated at 1550 nm by means of a CW laser from Exfo modulated thanks to a 14-Gbit.s<sup>-1</sup> pulse-pattern generator (PPG from Anritsu Corporation). Two LiNbO<sub>3</sub> intensity modulators from Ixblue photonics (IM1 and IM2) are subsequently cascaded in order to improve the extinction-ratio (ER) of the generated piston pulses. In this way, an ER higher than 40 dB is achieved, thus preventing any spurious interference between the piston pulse and the residual background<sup>17,22</sup>. This pulse train is then amplified by means of a 33-dBm Erbium doped fiber amplifier (EDFA from Manlight) and used as piston pump beam whose power can be continuously tuned thanks to a programmable variable optical attenuator (Exfo), thus ensuring an efficient stability of the setup, especially on polarization states. The probe wave consists of a 5-mW CW landscape which can be a simple replica of the initial 1550-nm signal to ensure a perfect velocity matching (null walk-off configuration,  $\delta = 0$  in Eq. (1)) or a distinct CW generated from a second external cavity laser from Exfo so as to induce a variable velocity mismatch between the piston and probe signals. Piston and probe waves are then orthogonally polarized by means of two polarization controllers, combined in a first polarization beam splitter (PBS), and injected into a 13-km-long dispersion compensating fiber (DCF from OFS). The DCF fiber spool is characterized by a normal chromatic dispersion  $D = -130$  ps.nm<sup>-1</sup>.km<sup>-1</sup> at 1550 nm ( $\beta_2 = 166$  ps<sup>2</sup>.km<sup>-1</sup>), an attenuation parameter  $\alpha = 0.4$  dB.km<sup>-1</sup> and a nonlinear Kerr coefficient  $\gamma' = 5.5$  W<sup>-1</sup>.km<sup>-1</sup>. At the output of the system, the piston pulse beam and the CW probe are polarization demultiplexed using a second PBS and characterized both in the temporal and spectral domains by means of two high-speed photodetectors from U2T connected to a dual-channel 70-GHz electrical sampling oscilloscope (Agilent DCA 86118 A) and an optical spectrum analyzer (OSA Yokogawa AQ6370), respectively. Note that before temporal detection, a tunable optical bandpass filter from Exfo may be inserted in such a way to carry



out a spectral-temporal analysis (see Fig. 5d). Finally, the entire experimental platform was automatically controlled from a single computer, which enables us to accumulate up to 150 measurements in a very short time scale, providing perfect stability whilst mapping the entire shock dynamics.

### Data availability

The data that support the findings of this study are available from the corresponding author upon reasonable request.

Received: 3 June 2019; Accepted: 10 October 2019;

Published online: 06 November 2019

### References

- Coleman, T. A., Knupp, K. R. & Herzmann, D. The spectacular undular bore in Iowa on 2 October 2007. *Mon. Wea. Rev.* **137**, 495 (2009).
- Chanson, H. *Tidal bores Aegir, Eagre, Mascaret, Proroca: Theory and Observations* (World Scientific, 2012).
- Clarke, R. H., Smith, R. K. & Reid, D. G. The Morning Glory of the gulf of Carpentaria: an atmospheric undular bore. *Mon. Wea. Rev.* **109**, 1726 (1981).
- Hodges, S. & Carverhill, A. Quasi-mean reversion in an efficient stock market; the characterization of economic equilibria which support Black–Scholes option pricing. *Econom. J.* **103**, 395 (1993).
- Whitham, G. B. *Linear and Nonlinear Waves* (Wiley, 1974).
- El, G. A. & Hoefler, M. A. Dispersive shock waves and modulation theory. *Phys. D* **333**, 11–65 (2016).
- Bendahmane, A. et al. Experimental Realization of Riemann Problem in Nonlinear Fiber Optics. In *Nonlinear Optics (NLO)*. paper NTu1A.4 (Optical Society of America, 2019).
- Rolley, E., Guthmann, C. & Pettersen, M. S. The hydraulic jump and ripples in liquid helium. *Phys. B* **394**, 46–55 (2007).
- Hoefler, M. A. et al. Dispersive and classical shock waves in Bose-Einstein condensates and gas dynamics. *Phys. Rev. A* **74**, 023623 (2006).
- Rothenberg, J. E. & Grischkowsky, D. Observation of the formation of an optical intensity shock and wave-breaking in the nonlinear propagation of pulses in optical fibers. *Phys. Rev. Lett.* **62**, 531–534 (1989).
- Wan, W., Jia, S. & Fleischer, J. W. Dispersive superfluid-like shock waves in nonlinear optics. *Nat. Phys.* **3**, 46–51 (2007).
- Jia, S., Wan, W. & Fleischer, J. W. Forward four-wave mixing with defocusing nonlinearity. *Opt. Lett.* **32**, 1668 (2007).
- Ghofraniha, N., Gentilini, S., Folli, V., DelRe, E. & Conti, C. Shock waves in disordered media. *Phys. Rev. Lett.* **109**, 243902 (2012).
- Wetzel, B. et al. Experimental generation of Riemann waves in optics: a route to shock wave control. *Phys. Rev. Lett.* **117**, 073902 (2016).
- Fatome, J., Finot, C., Millot, G., Armario, A. & Trillo, S. Observation of optical undular bores in multiple four-wave mixing. *Phys. Rev. X* **4**, 021022 (2014).
- Varlot, B., Wabnitz, S., Fatome, J., Millot, G. & Finot, C. Experimental generation of optical flatonic pulses. *Opt. Lett.* **38**, 3899–3902 (2013).
- Xu, G. et al. Shock wave generation triggered by a weak background in optical fibers. *Opt. Lett.* **41**, 2656–2659 (2016).
- Xu, G., Conforti, M., Kudlinski, A., Mussot, A. & Trillo, S. Dispersive dam-break flow of a photon fluid. *Phys. Rev. Lett.* **118**, 254101 (2017).
- Trillo, S. & Valiani, A. Hydrodynamic instability of multiple four-wave mixing. *Opt. Lett.* **35**, 3967–3969 (2010).
- Kodama, Y. & Wabnitz, S. Analytical theory of guiding-center nonreturn-to-zero and return-to-zero signal transmission in normally dispersive nonlinear optical fibers. *Opt. Lett.* **20**, 2291–2293 (1995).
- Wabnitz, S., Finot, C., Fatome, J. & Millot, G. Shallow water rogue wavetrains in nonlinear optical fibers. *Phys. Lett. A* **377**, 932–939 (2013).
- Parriaux, A. et al. Spectral broadening of picosecond pulses forming dispersive shock waves in optical fibers. *Opt. Lett.* **42**, 3044–3047 (2017).
- Kamchatnov, A. M., A., G. & Kraenkel, R. A. Dissipationless shock waves in Bose-Einstein condensates with repulsive interaction between atoms. *Phys. Rev. A* **69**, 063605 (2004).
- Dutton, Z., Budde, M., Slowe, C. & Hau, L. V. Observation of quantum shock waves created with ultra-compressed slow light pulses in a Bose-Einstein condensate. *Science* **293**, 663 (2001).
- Taylor, R. J., Baker, D. R. & Ikezi, H. Observation of collisionless electrostatic shocks. *Phys. Rev. Lett.* **24**, 206–209 (1970).
- Joseph, J. A., Thomas, J. E., Kulkarni, M. & Abanov, A. G. Observation of shock waves in a strongly interacting fermi gas. *Phys. Rev. Lett.* **106**, 150401 (2011).
- Ivanov, S. K., Kamchatnov, A. M. & Pavloff, N. Solution of the Riemann problem for polarization waves in a two-component Bose-Einstein condensate. *Phys. Rev. E* **96**, 062202 (2017).
- Ivanov, S. K. & Kamchatnov, A. M. Simple waves in a two-component Bose-Einstein condensate. *Phys. Rev. E* **97**, 042208 (2018).
- Barsi, C., Wan, W., Jia, S. & Fleischer, J. W. *Nonlinear Photonics and Novel Optical Phenomena* (Springer, 2012).
- Stoughton, R. Measurements of small caliber ballistic shock waves in air. *J. Acoust. Soc. Am.* **102**, 781–786 (1997).
- Hoefler, M. A., Ablowitz, M. J. & Engels, P. Piston dispersive shock wave problem. *Phys. Rev. Lett.* **100**, 084504 (2008).
- Mossman, M. E., Hoefler, M. A., Julien, K., Kevrekidis, P. G. & Engels, P. Dissipative shock waves generated by a quantum-mechanical piston. *Nat. Commun.* **9**, 4665 (2018).
- El, G. A., Gammal, A. & Kamchatnov, A. M. Generation of oblique dark solitons in supersonic flow of Bose-Einstein condensate past an obstacle. *Nucl. Phys. A* **790**, 771c–775c (2007).
- El, G. A., Kamchatnov, A. M., Khodorovskii, V. V., Annibale, E. S. & Gammal, A. Two-dimensional supersonic nonlinear Schrödinger flow past an extended obstacle. *Phys. Rev. E* **80**, 046317 (2009).
- El, G. A. & Kamchatnov, A. Spatial dispersive shock waves generated in supersonic flow of Bose-Einstein condensate past slender body. *Phys. Lett. A* **350**, 192–196 (2006).
- Rothenberg, J. E. Observation on the buildup of modulational instability from wave-breaking. *Opt. Lett.* **16**, 18–20 (1991).
- Agrawal, G. P. *Nonlinear Fiber Optics, Fourth Edition* (Academic Press, 2006).
- Wai, P. K. A., Menyuk, C. R. & Chen, H. H. Stability of solitons in randomly varying birefringent fibers. *Opt. Lett.* **16**, 1231–1233 (1991).
- Marcuse, D., Menyuk, C. R. & Wai, P. K. A. Application of the Manakov-PMD equation to studies of signal propagation in optical fibers with randomly varying birefringence. *J. Light. Technol.* **15**, 1735–1746 (1997).
- Anderson, D., Desaix, M., Lisak, M. & Quiroga-Teixeiro, M. L. Wave-breaking in nonlinear optical fibers. *J. Opt. Soc. Am. B* **9**, 1358–1361 (1992).
- Finot, C., Kibler, B., Provost, L. & Wabnitz, S. Beneficial impact of wave-breaking on coherent continuum formation in normally dispersive nonlinear fibers. *J. Opt. Soc. Am. B* **25**, 1938–1948 (2008).
- Zeytunyan, A. et al. Nonlinear-dispersive similariton of passive fiber. *J. Eur. Opt. Soc. Rap. Public.* **4**, 09009 (2009).
- Castelló-Lurbe, D., Andrés, P. & Silvestre, E. Dispersion-to-spectrum mapping in nonlinear fibers based on optical wave-breaking. *Opt. Express* **21**, 28550–28558 (2013).
- Mahjoubfar, A. et al. Time stretch and its applications. *Nat. Photon.* **11**, 341 (2017).
- Iakushev, S. O., Shulika, O. V. & Sukhoivanov, I. A. Passive nonlinear reshaping towards parabolic pulses in the steady-state regime in optical fibers. *Opt. Commun.* **285**, 4493–4499 (2012).
- Islam, M. N., Mollenauer, L. F., Stolen, R. H., Simpson, J. R. & Shang, H. T. Cross-phase modulation in optical fibers. *Opt. Lett.* **12**, 625–627 (1987).
- Treacy, E. B. Measurement and interpretation of dynamic spectrograms of picosecond light pulses. *J. Appl. Phys.* **42**, 3848–3858 (1971).
- Linden, S., Giessen, H. & Kruhl, J. XFROG-A new method for amplitude and phase characterization of weak ultrashort pulses. *Phys. Stat. Sol.* **206**, 119–124 (1998).
- Niedzwiecki, A. & Ribner, H. S. Subjective loudness of N-wave sonic booms. *J. Acoust. Soc. Am.* **64**, 1617–1621 (1978).
- Hammer, C., Chang, J. J., Engels, P. & Hoefler, M. A. Generation of dark-bright soliton trains in superfluid-superfluid counterflow. *Phys. Rev. Lett.* **106**, 065302 (2011).
- Frisquet, B. et al. Polarization modulation instability in a Manakov fiber system. *Phys. Rev. A* **92**, 053854 (2015).
- Congy, T., Kamchatnov, A. & Pavloff, N. Dispersive hydrodynamics of nonlinear polarization waves in two-component Bose-Einstein condensates. *SciPost Phys.* **1**, 006 (2016).

### Acknowledgements

All the experiments were performed on the PICASSO platform in ICB. We also thank A. Picozzi, and D. Castelló-Lurbe for fruitful discussions, in particular for the calculation of the wave breaking distance. J.F. acknowledges the financial support from the European Research Council (Grant Agreement 306633, PETAL project), the FEDER, the DRRT, the Conseil Régional de Bourgogne Franche-Comté (International Mobility Program) which has allowed him to visit The University of Auckland to contribute to this work. C.F. and G.M. acknowledge support from Institut Universitaire de France (IUF). We also thank EUR EIPHI graduate school (ANR-17-EURE-0002) and the ISITE-BFC (ANR-15-IDEX-0003). M.E. acknowledges support from the Rutherford Discovery Fellowships and Marsden Funds administered by the Royal Society of New Zealand.

### Author contributions

J.F. and C.F. designed the experiment. J.F. and J.N. carried out the experiments. J.F., C.F., J.N., G.X., M.E., and G.M. participated in the analysis of the results. J.F., C.F., J.N., and G.X. performed numerical simulations and theoretical description of the process. J.F., C.F., and M.E. wrote the paper. All the authors participated to improve the paper. J.F. supervised the project.

### Competing interests

The authors declare no competing interests.

### Additional information

**Supplementary information** is available for this paper at <https://doi.org/10.1038/s42005-019-0241-6>.

**Correspondence** and requests for materials should be addressed to J.F.

**Reprints and permission information** is available at <http://www.nature.com/reprints>

**Publisher's note** Springer Nature remains neutral with regard to jurisdictional claims in published maps and institutional affiliations.



**Open Access** This article is licensed under a Creative Commons Attribution 4.0 International License, which permits use, sharing, adaptation, distribution and reproduction in any medium or format, as long as you give appropriate credit to the original author(s) and the source, provide a link to the Creative Commons license, and indicate if changes were made. The images or other third party material in this article are included in the article's Creative Commons license, unless indicated otherwise in a credit line to the material. If material is not included in the article's Creative Commons license and your intended use is not permitted by statutory regulation or exceeds the permitted use, you will need to obtain permission directly from the copyright holder. To view a copy of this license, visit <http://creativecommons.org/licenses/by/4.0/>.

© The Author(s) 2019